




Black phosphorus unipolar transistor, memory, and photodetector

Arun Kumar^{1,*} , Loredana Viscardi¹, Enver Faella^{1,2}, Filippo Giubileo², Kimberly Intonti¹, Aniello Pelella^{1,2}, Stephan Slezione³, Osamah Kharsah³, Marika Schleberger³, and Antonio Di Bartolomeo^{1,2,*}

¹Department of Physics, University of Salerno, Via Giovanni Paolo II, 84084 Fisciano, Salerno, Italy

²CNR-SPIN, Via Giovanni Paolo II, 84084 Fisciano, Salerno, Italy

³Fakultät für Physik and CENIDE, Universität Duisburg-Essen, Lotharstrasse 1, 47057 Duisburg, Germany

Received: 2 September 2022

Accepted: 9 January 2023

Published online:
22 January 2023

© The Author(s) 2023

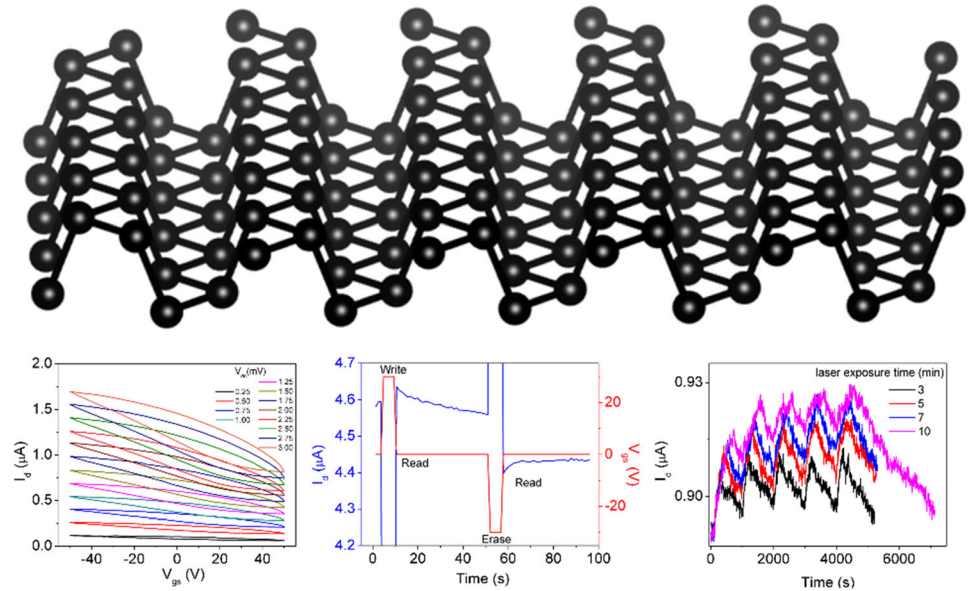
ABSTRACT

We report the fabrication, electrical, and optical characterizations of few-layered black phosphorus (BP)-based field-effect transistor (FET). The fabricated device exhibits a p-type transport with hole mobility up to $175 \text{ cm}^2 \text{ V}^{-1} \text{ s}^{-1}$ at $V_{ds} = 1 \text{ mV}$. The transfer characteristics show a large hysteresis width that depends linearly on the gate voltage and decreases with the increasing drain bias. The fabricated device also ensures a non-volatile charge-trap memory behaviour, with a stable and long retention time. The material's photodetection capabilities enhance the functionality of the device making it controllable by light. The photocurrent was observed to be linearly increasing with the light incident power and exposure time. As a photodetector, the transistor reaches a responsivity and detectivity up to 340 mA W^{-1} and 6.52×10^{11} Jones under white light at 80 mW , respectively. Time-resolved measurements provide evidence of a long single exponential decay process through deep intra-gap states. Our results highlight the potential of a few layers BP as a nanomaterial for field-effect, memory, and optoelectronic devices.

Handling Editor: Pedro Camargo.

Address correspondence to E-mail: akumar@unisa.it; adibartolomeo@unisa.it

GRAPHICAL ABSTRACT



Introduction

Two-dimensional (2D) transition metal dichalcogenides (TMDs) having a direct band gap, for example MoS_2 , WS_2 , and MoSe_2 , have generated a significant rise in the scientific research and interest for their utilization as the semiconducting channel materials for novel nanoelectronics and optoelectronics [1–9]. Besides TMDs and graphene, recently, a new class of 2D materials from single elements, such as black phosphorus (BP), arsenene, silicene, are being investigated for next-generation electronic devices [10–19]. With longer stability, high carrier mobility, and large on/off current ratios, they have attracted tremendous attention in researching their electrical properties [20–23]. Considering that the intrinsic structural defects and the interfacial charge impurities induced high electron doping, most of the 2D semiconductors exhibit n-type conduction behaviour [24–26]. On the other hand, p-type conduction behaviour in the 2D semiconductor materials is largely affected due to the Fermi level pinning at the metal–2D semiconductor materials interface which induces a large Schottky Barrier height for the hole injection [12, 27–30].

In 2014, black phosphorus (BP) again gained scientific interest with a promising path for various applications based on this material [31–35]. Due to its direct and thickness-dependent band gap of 0.3–2.0 eV and high carrier mobility of more than $1000 \text{ cm}^2\text{V}^{-1} \text{ s}^{-1}$ in comparison to various transition metal dichalcogenides [10, 11], BP quickly became the subject of many research efforts. Because of the Fermi level pinning at the contacts, and the small band gap, most BP transistors reported in the literature show n-type or ambipolar electrical transport properties [25, 36–39]. Conversely, reports about p-type BP transistors are scarce, which not only limits the fundamental understanding but also the broad integration of BP in technological applications, especially in complementary metal-oxide semiconductor (CMOS) circuits.

Among various BP channel-based functional devices, non-volatile memory realization is considered one of the significant outcomes [40, 41]. Most memories based on non-volatile FET utilize a charge-trapping layer to collect and retain the electric charge induced by the gate pulse [40]. Additionally, non-volatile memory based on BP also holds great promise for future flexible and transparent devices

because of the mechanical flexibility and tuneable electronic properties [38, 42].

Further, both high photoresponsivity and low dark current can be achieved by only a few photoconductive type photodetectors depending on a minority of semiconductors. In recent years, the research focus has been to lower the dark current and improve the photoelectric performance of photodetectors, heterojunctions, as well as of p–n heterojunctions. As a part of the p–n heterojunction in photoelectric devices, p-type semiconductor materials exhibit prominent and irreplaceable functions [7, 24, 43, 44]. Moreover, BP exhibits a strong light-matter interaction with light in the visible-to-infrared range, which makes this material a promising candidate for photodetector [45, 46] and photovoltaics applications [47].

However, due to high instability and easy degradation of the BP under ambient conditions [48], its implication is still limited in practical applications. To avoid the BP layer deterioration under air exposure, previously, we have shown that the utilization of a protective poly(methyl methacrylate) (PMMA) layer, deposited over the top of a BP channel, would not alter the electrical properties of the fabricated device [41].

In the present work, the electrical properties of unipolar p-type BP transistors, obtained using high-work function Ni metal contacts, are explored. The transfer characteristics show a large hysteresis that depends linearly on the gate voltage and decreases with the drain bias. We exploit such a property to realize BP-based non-volatile memories, resulting in good endurance, and high retention time. We perform photodetection studies evidencing a long decay photocurrent, resulting from the trapping of carriers excited in the BP layer under the light illumination. More importantly, we demonstrate the linear behaviour of the fabricated device under varying incident laser powers and exposure times, which makes it suitable for photodetection applications.

Materials and methods

A bulk BP single crystal (by Smart Elements) was used for mechanically exfoliating the few layers BP thin flakes with an adhesive tape. The exfoliated flakes were transferred onto the 90 nm thick SiO₂/p+ Si substrate. A detailed explanation of the device fabrication procedure can be found in our previously

published work [41]. Before the electrical measurements, the PMMA layer was separated by simply keeping the device in acetone for 2 h and then cleaning it with isopropanol. The fabricated BP device was back-gated with a silver (Ag) paste onto the heavily doped p + Si substrate. Atomic force microscopy (AFM) (Nanosurf AG, Liestal, Switzerland) was used to measure the thickness of BP flake.

Electrical measurements were performed in a two-probe configuration mode using a Janis ST-500 probe station connected with a Keithley 4200 SCS (semiconductor characterization system), having a current and voltage sensitivity of about 1 pA and 2 μV, respectively. All the measurements were carried out at 2 mbar pressure and room temperature. To investigate the photoresponse of the BP flakes, a white laser source, (by NKT Photonics Super Compact), with an operating range between 450 and 2400 nm, at 100% of the full incident power of 80 mW, was employed.

Results and discussion

PMMA protective capping layer on the BP was removed, immediately before the electrical measurements in vacuum. Figure 1a illustrates a schematic structure of the fabricated back-gated BP device with Ni/Au metal contacts. The BP flake is stacked on the SiO₂/p + Si substrate, with the two metal contacts made up of 70 nm Au on the top of 10 nm Ni over the flake. p + doped Si back-gated electrode was used for applied gate bias. During the photodetection measurements, a white laser is incident from the top of the device. Figure 1b displays an optical micrograph of the fabricated device, of which two inner contacts were used for measurements. We used an AFM to measure the thickness of the BP flake. AFM measurements (Fig. 1c) were performed in the air after electrical measurements, which degrades the flakes. The measured flake thickness on the fabricated device is about 20 nm.

We first carried out two-terminal transport measurements between the source and drain leads. Figure 2a shows the output characteristics, i.e. the drain current (I_d) as a function of the voltage drop between the two inner contacts (V_{ds}), with the gate-source voltage (V_{gs}) as the control parameter. A linear performance, that is not affected by the gate bias, can be observed, indicating ohmic contacts and the absence of

Figure 1 **a** Schematic illustration of the BP/SiO₂ fabricated device structure (not on scale), **b** optical image of the fabricated device, and **c** AFM image, and corresponding height profile along the marked dashed white line.

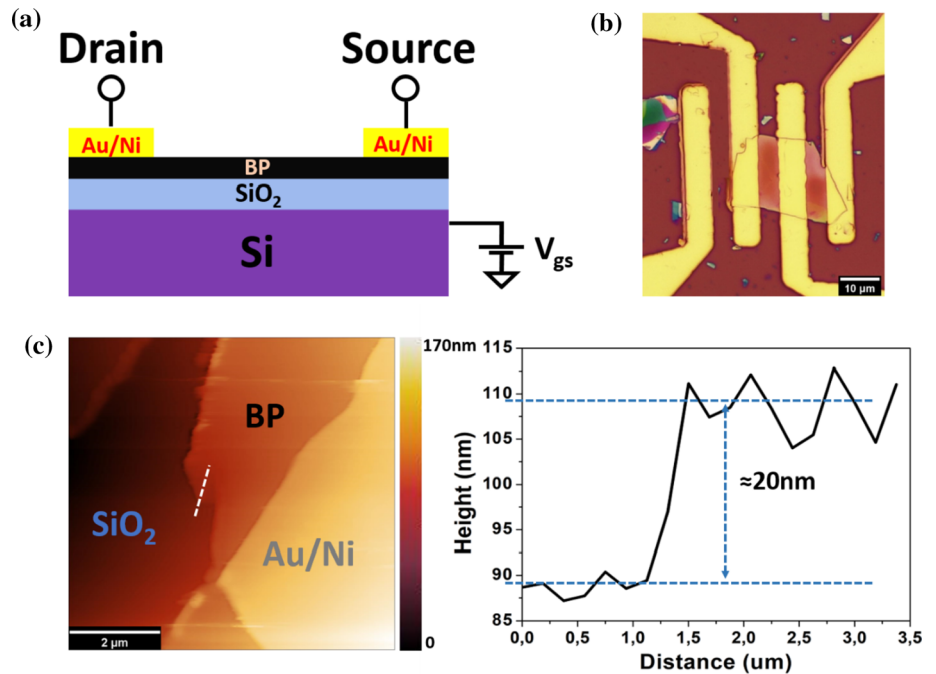
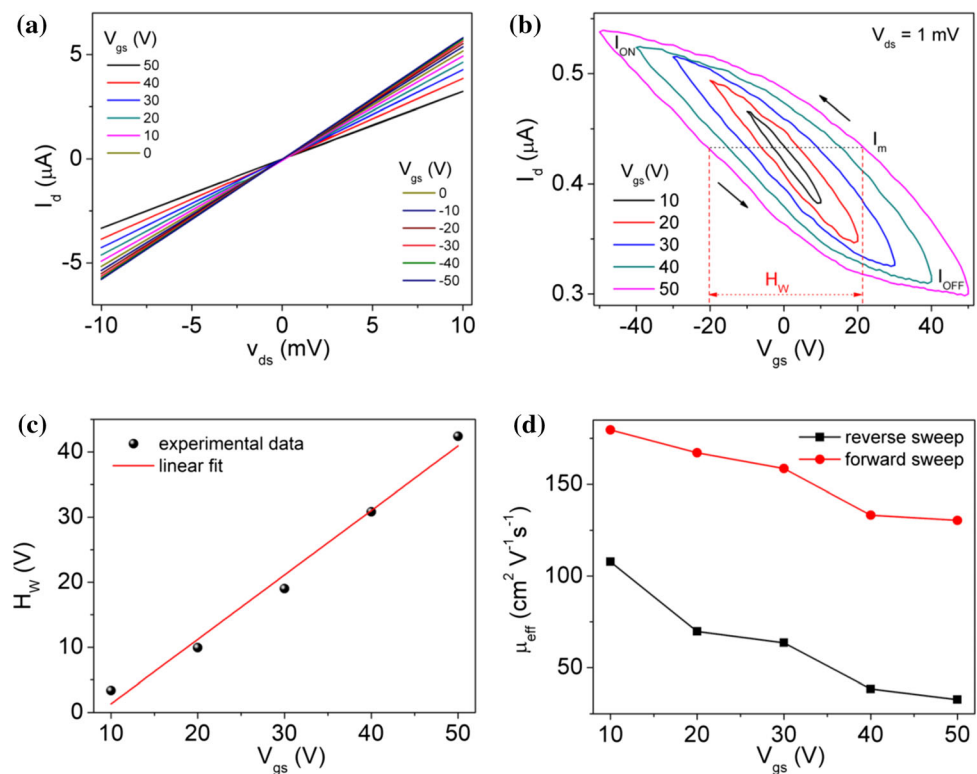


Figure 2 **a** Output, **b** transfer characteristics of the fabricated device, **c** hysteresis width at $I_m = (I_{on} + I_{off})/2$, and **d** calculated mobility as a function of the gate voltage.



current saturation over the explored V_{ds} range. An increase in the channel current at the negative gate bias shows that the device is typical of a p-type. Figure 2b shows the transfer characteristics of the device under a drain bias of 1 mV over growing loops of the gate voltage, up to $-50\text{ V} \leq V_{gs} \leq 50\text{ V}$. We avoided applying

higher gate voltages to prevent gate oxide damage. The transfer characteristics confirm the p-type behaviour of the transistor, confirming that the Fermi level of the fabricated BP transistor with Ni contacts is near the valence band of BP flake. Indeed, to enhance device performance and modulate the BP transistor type,

several metal contacts have been utilized. It has been reported that low-work function metals like scandium (Sc), aluminium (Al), or titanium (Ti) produced n-type behaviour, while high-work function metals like nickel (Ni), platinum (Pt), and palladium (Pd) were more likely to exhibit the p-type feature [49]. The ultimate polarity of the transistor is significantly influenced by both the work function of the metal contact and the thickness of the BP channel because the bandgap of BP is thickness-dependent. We also note that the transistor is in the on-state at zero gate voltage due to the doping effect of charges trapped at the BP/SiO₂ interface and to residual adsorbates, such as O₂ and H₂O molecules, which act as p-dopant. Next, a low modulation in the current as well as an enhancement in the hysteresis width as a function of the V_{gs} sweeping range was observed. The low modulation of the current is because of the low energy band gap of the multilayers BP as we did not apply pressure or strain, which could help in increasing the band gap [50–55]. Furthermore, the free carriers in the bottom layers of the BP flake were induced by the applied gate electric field, while in this situation, the top layers still provide finite conduction in the off state, lowering the modulation in the drain current.

Figure 2c demonstrates that the hysteresis width, defined as the V_{gs} difference corresponding to the average current, $I_m = (I_{on} + I_{off})/2$ between the highest (I_{on}) and lowest (I_{off}) currents at the extreme of the gate voltage range (see Fig. 2b), is a linear function of V_{gs} . The large hysteresis width up to about 45 V is due to the trapped charges at the interface of BP/SiO₂ and the intrinsic BP defects [56, 57]. The linear dependence of the hysteresis width on V_{gs} confirms that charge storage occurs across the SiO₂ capacitor. Adsorbates, which usually play an important role in hysteresis, are expected to have here minor effects as the measurements were performed in vacuum [58, 59]. The following equation was used for calculating the charge carrier mobility of the BP film FETs,

$$\mu = \frac{L}{WC_{ox}V_{ds}} \frac{dI_d}{dV_{gs}}$$

where L and W are the channel length and width, respectively, and dI_d/dV_{gs} is the maximum slope of the transfer curves.

We inferred two-terminal field-effect hole mobilities (see Fig. 2d), in the reverse and forward bias direction, with maximum values of 175 and 110 cm² V⁻¹ s⁻¹ at

$V_{ds} = 1$ mV, respectively. The different mobilities in the two directions and the dependence on V_{gs} can be ascribed to the interfacial trap states which are differently populated. We note that the observed hole mobility is higher than our previously reported value [41] as well as from other reports on thin BP [60, 61] and the recently reported p-type violet phosphorus [62] at room temperature.

Figure 3a shows the transfer curves of the fabricated BP device with V_{ds} ranging from 0.25 to 3 mV. The measurements do not exhibit any ambipolar behaviour in the ± 50 V range, but a strong unipolar p-type conduction behaviour. Also, we note in Fig. 3b, a decrease in the hysteresis width as a function of increasing V_{ds} . Such a trend points towards the role of the intrinsic traps in the BP channel, which add to the ones present at the BP/SiO₂ interface in the generation of hysteresis. Lower V_{ds} facilitates charge trapping in the channel and results in wider hysteresis. The inset of Fig. 3b shows that both I_{on} and I_{off} currents depend linearly on V_{ds} , confirming the device in the linear (triode) region over the investigated V_{gs} and V_{ds} voltages.

Figure 4a shows the performance of the fabricated BP device, measured over a series of $V_{gs} = \pm 30$ V pulses, while the I_d current is recorded over time, at 2 mbar pressure. When the gate pulse is in the high positive or negative state, the channel current increases or decreases rapidly, and trap states get filled or emptied by positive charge. After that, two states with different current values can be defined at $V_{gs} = \pm 0$ V, corresponding to the write and the read state of a memory device, respectively. The transient behaviour, in Fig. 4b, after a positive and a negative gate pulse shows that I_d stabilizes at two distinct values that stay well separated for a few dozen seconds, demonstrating the non-volatile characteristic of the memory. The retention execution shows that the trapped charges are preserved without a loss of charge. Most of the memories relying on a charge-trapping mechanism do not achieve such long charge retention because of back tunnelling charge loss, opposite type carrier injection or charge redistribution in defects [63]. Conversely, the endurance and the charge retention [64], shown in Fig. 4a, b, respectively, highlight the potential use of BP transistors for non-volatile memory technology.

To explore the photoresponse in the fabricated BP device, we examined the current–time characteristics for different light incident powers and exposure

Figure 3 **a** Transfer characteristics and **b** hysteresis width (inset: I_{ON} and I_{OFF} values with a linear fit) of the fabricated BP FET at variable V_{ds} .

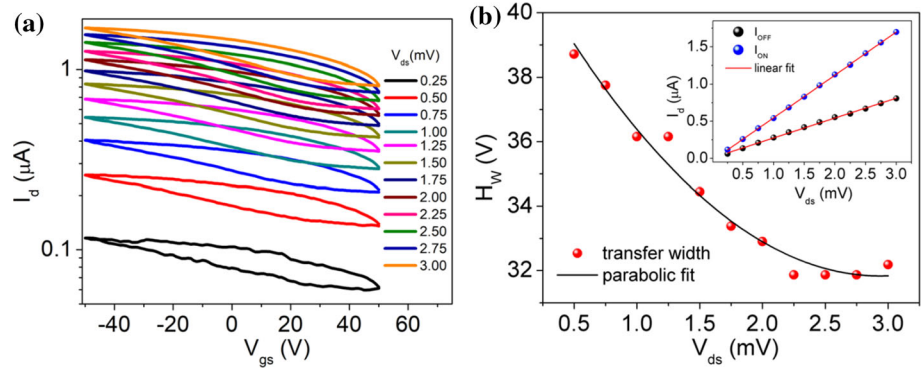


Figure 4 **a** Channel current (I_d) recorded under gate pulses (V_{gs}) at ± 30 V showing repeated write–read–erase–read cycles, and **b** single write–read–erase–read cycle of the BP-based memory device.

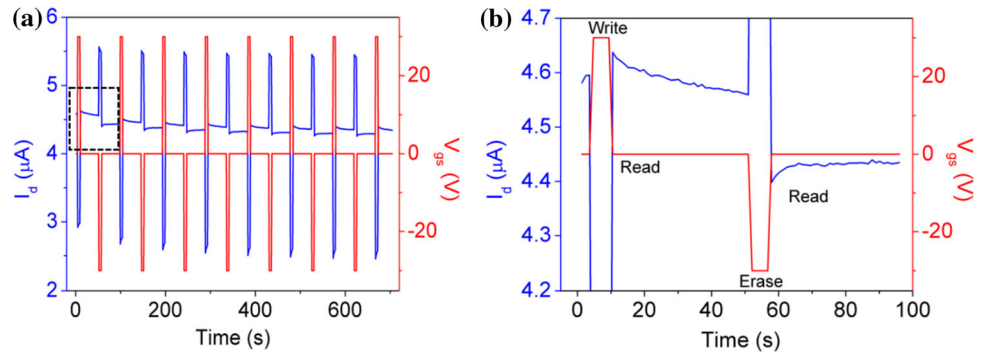
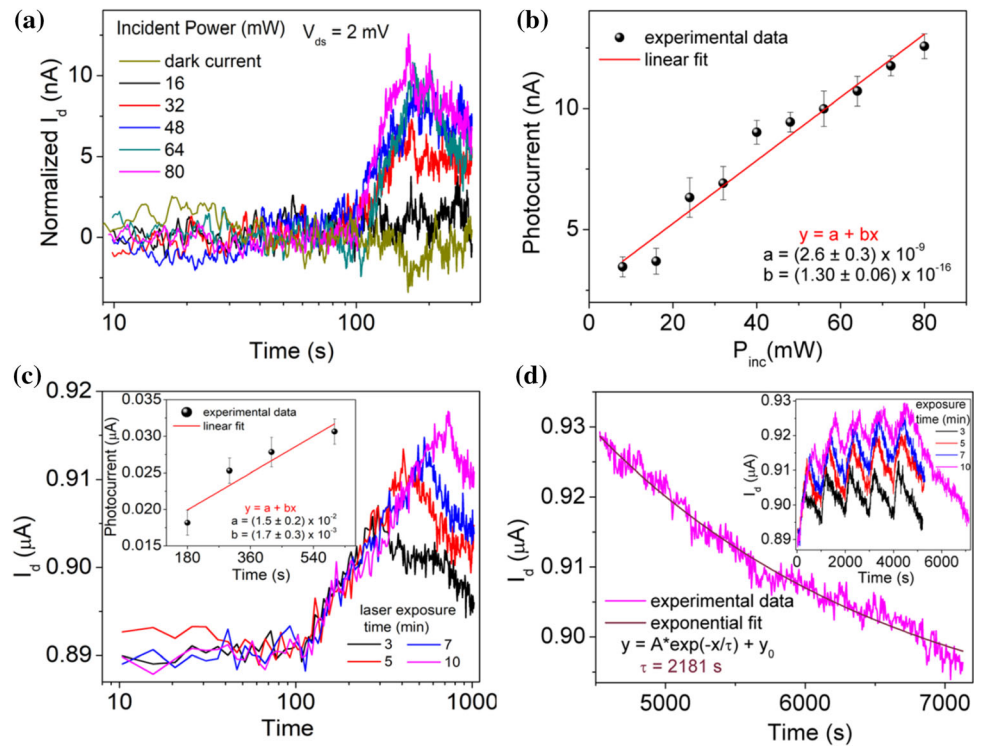


Figure 5 **a** Normalized current in dark–light–dark conditions at various laser incident powers (only a subset of curves is shown), at fixed $V_{gs} = 0$ V and $V_{ds} = 2$ mV, **b** photocurrent versus laser incident power, **c** current at various laser exposure times (inset: photocurrent versus exposure time), and **d** current decay and exponential fit of the current after 10 min laser exposure time (inset: current at various exposure times) of fabricated BP FET device.



times. The measurements were carried out at 2 mbar pressure, thus the noise in the experimental data could be due to the presence of residual volatile

compounds or water vapour in the surrounding environment. Figure 5a shows the device normalized current as a function of the laser incident power, P_{inc} ,

Table 1 Comparison of recently reported representative photodetectors based on 2D materials

Device	Applied bias (V)	Responsivity (AW^{-1})	Detectivity (Jones)	References
BP	2×10^{-3}	340×10^{-3}	6.52×10^{11}	This work
BP/MoSe ₂	– 0.25 V	3.2×10^{-3}	1.4×10^9	[70]
Violet Phosphorus	1 V	10×10^{-3}	–	[62]
MoS ₂	2 V	1.10×10^{-3}	3.86×10^{10}	[71]
WSe ₂ , at 400 C	–	2.2×10^6	1.6×10^{13}	[72]
PtSe ₂	–	8.06	4.78×10^{13}	[73]
ReS ₂ /ReSe ₂	–	0.66–126.56	1.76×10^{11}	[74]

indicating an increase with increasing laser intensity, at fixed $V_{ds} = 2 \text{ mV}$ and $V_{gs} = 0 \text{ V}$, respectively. The highest photocurrent was observed to be about $0.86 \mu\text{A}$, with a laser incident power of 80 mW . Figure 5b demonstrates the corresponding linear behaviour between the photocurrent and the laser intensity. A linear dependence is found also when the current is plotted as a function of the laser exposure time as shown in Fig. 5c, and its inset. The linear response of the photodetector enhances the time-resolved photocurrent as the decay time increases [65], and we observed this phenomenon in our device also discussed in the next section. The observed linear behaviour is very promising for practical photodetection applications.

We evaluate the photoresponsivity (R) of the device through the relation, $R = (I_{\text{Light}} - I_{\text{Dark}}) / P_{\text{inc}}$, where I_{Light} and I_{Dark} are the current under illumination and in dark recorded at $V_{ds} = 2 \text{ mV}$ and $V_{gs} = 0 \text{ V}$, respectively, P_{inc} is the laser power incident over the device area. Given the optical power of 80 mW at the surface of samples and an effective area of $100 \mu\text{m}^2$, we obtained $R \approx 340 \text{ mA W}^{-1}$. The calculated responsivity is higher than that found for the BP of similar thickness [66], and much higher than the previously reported for other BP devices [67–70].

Next, from the experimental data, we calculated the detectivity (D) of the fabricated device, where D is defined as

$$D = \frac{\sqrt{SR}}{\sqrt{2eI_d}}$$

where S is the effective area, R is responsivity, e is the electron charge, and I_d is the dark current. The calculated detectivity for the $100 \mu\text{m}^2$ BP channel is 6.52×10^{11} Jones at room temperature. The obtained detectivity is larger than most BP-based photodetectors reported. The obtained high responsivity and detectivity at low power consumption levels are desirable, as they suggest the use of BP channel-

based devices where the light is in scarceness. A comparison of the responsivity and detectivity with the recently published reports on the 2D materials is summarized in Table 1.

The slow rise and decay time of the photocurrent indicates that deep intra-gap states play a dominant role in the photoresponse of the BP device. Otherwise stated, the photocurrent seems to be dominated by charge excitation from trap sites rather than by electron–hole pair generation [75]. Analogously, when the light is switched off, carrier trapping seems to be the main mechanism that makes the current go back to its starting value. The decay process presents a single exponential decay character and can be fitted by an empirical equation stated as

$$y = A \times \exp(-x/\tau) + y_0$$

as shown in Fig. 5d. The need for a single characteristic time τ points to a single type of trap that dominates the decay process with a characteristic time $\tau \sim 35 \text{ min}$ (a similar analysis leads to a $\tau \sim 10 \text{ min}$ for the rise time). We remark that the prolonged photo carrier lifetime could be exploited for optical memory [76], light-emitting and lasing applications [77].

Conclusions

In summary, we have explored a BP-based field-effect transistor with Au/Ni contacts. The device shows p-type conduction behaviour with hole mobility up to $175 \text{ cm}^2 \text{ V}^{-1} \text{ s}^{-1}$. The transfer characteristics exhibit hysteresis that is modulated by the gate and the drain bias as a contribution of both extrinsic and intrinsic trap states. Hysteresis has been exploited to achieve the write and erase state of a memory device with long endurance and retention time. A photocurrent, corresponding to a responsivity of 340 mA W^{-1} and detectivity of about

6.52×10^{11} Jones, with a linear dependence on the light incident power and exposure time has been reported, showing promises for practical applications in photodetection. The slow, single exponential rise and decay time of the photocurrent indicates the dominant role of one type of trap and can be exploited to extend the functionality of the device to include optical memory effects.

Acknowledgements

Authors would like to acknowledge A. Lorke and the clean room staff of the University of Duisburg-Essen for access to the clean room facility.

Funding

Open access funding provided by Università degli Studi di Salerno within the CRUI-CARE Agreement. Arun Kumar and A. Di Bartolomeo acknowledge the European Union's REACT-EU PON Research and Innovation 2014–2020, Italian Ministerial Decree 1062/2021 Project. St.S. and M.S. acknowledge financial support from the BMBF (Project 05K16PG1).

Declarations

Conflict of interest The authors declare that they have no conflict of interest.

Open Access This article is licensed under a Creative Commons Attribution 4.0 International License, which permits use, sharing, adaptation, distribution and reproduction in any medium or format, as long as you give appropriate credit to the original author(s) and the source, provide a link to the Creative Commons licence, and indicate if changes were made. The images or other third party material in this article are included in the article's Creative Commons licence, unless indicated otherwise in a credit line to the material. If material is not included in the article's Creative Commons licence and your intended use is not permitted by statutory regulation or exceeds the permitted use, you will need to obtain permission directly from the copyright holder. To view a copy of this licence, visit <http://creativecommons.org/licenses/by/4.0/>.

References

- [1] Lopez-Sanchez O, Lembke D, Kayci M et al (2013) Ultrasensitive photodetectors based on monolayer MoS₂. *Nat Nanotechnol* 8(8):497–501. <https://doi.org/10.1038/nnano.2013.100>
- [2] Mak KF, McGill KL, Park J, McEuen PL (2014) The valley hall effect in MoS₂ transistors. *Science* (80-) 344:1489–1492
- [3] Kufer D, Konstantatos G (2015) Highly sensitive, encapsulated MoS₂ photodetector with gate controllable gain and speed. *Nano Lett* 15:7307–7313
- [4] Li F, Xu B, Yang W et al (2020) High-performance optoelectronic devices based on van der Waals vertical MoS₂/MoSe₂ heterostructures. *Nano Res* 13:1053–1059. <https://doi.org/10.1007/S12274-020-2743-7>
- [5] Khan AR, Lu T, Ma W et al (2020) Tunable optoelectronic properties of WS₂ by local strain engineering and folding. *Adv Electron Mater* 6:1901381. <https://doi.org/10.1002/AE.LM.201901381>
- [6] Choi J, Zhang H, Choi JH (2016) Modulating optoelectronic properties of two-dimensional transition metal dichalcogenide semiconductors by photoinduced charge transfer. *ACS Nano* 10:1671–1680
- [7] Zhang YJ, Onga M, Qin F et al (2018) Optoelectronic response of a WS₂ tubular p–n junction. *2D Mater* 5:035002. <https://doi.org/10.1088/2053-1583/AAB670>
- [8] Di Bartolomeo A (2020) Emerging 2D materials and their Van Der Waals heterostructures. *Nanomater* 10:579. <https://doi.org/10.3390/NANO10030579>
- [9] Grillo A, Passacantando M, Zak A et al (2020) WS₂ nanotubes: electrical conduction and field emission under electron irradiation and mechanical stress. *Small* 16:2002880. <https://doi.org/10.1002/SMLL.202002880>
- [10] Li L, Yu Y, Ye GJ et al (2014) (2014) Black phosphorus field-effect transistors. *Nat Nanotechnol* 9(9):372–377. <https://doi.org/10.1038/nnano.2014.35>
- [11] Xia F, Wang H, Jia Y (2014) Rediscovering black phosphorus as an anisotropic layered material for optoelectronics and electronics. *Nat Commun* 5(1):1–6. <https://doi.org/10.1038/ncomms5458>
- [12] Grillo A, Di Bartolomeo A (2021) A current–voltage model for double schottky barrier devices. *Adv Electron Mater* 7:2000979. <https://doi.org/10.1002/AELM.202000979>
- [13] Liang J, Hu Y, Zhang K et al (2021) 2D layered black arsenic-phosphorus materials: synthesis, properties, and device applications. *Nano Res* 15(15):3737–3752. <https://doi.org/10.1007/S12274-021-3974-Y>
- [14] Du J, Xia C, An Y et al (2016) Tunable electronic structures and magnetism in arsenene nanosheets via transition metal

- doping. *J Mater Sci* 51:9504–9513. <https://doi.org/10.1007/S10853-016-0194-Z/FIGURES/6>
- [15] Yuan JH, Zhang B, Song YQ et al (2019) Planar penta-transition metal phosphide and arsenide as narrow-gap semiconductors with ultrahigh carrier mobility. *J Mater Sci* 54:7035–7047. <https://doi.org/10.1007/S10853-019-03380-4/FIGURES/6>
- [16] Dhungana DS, Grazianetti C, Martella C et al (2021) Two-dimensional silicene-stanene heterostructures by epitaxy. *Adv Funct Mater* 31:2102797. <https://doi.org/10.1002/ADFM.202102797>
- [17] Di Bartolomeo A, Grillo A, Giubileo F et al (2020) Field emission from two-dimensional GeAs. *J Phys D Appl Phys* 54:105302. <https://doi.org/10.1088/1361-6463/ABCC91>
- [18] Glavin NR, Rao R, Varshney V et al (2020) Emerging applications of elemental 2D materials. *Adv Mater* 32:1904302. <https://doi.org/10.1002/ADMA.201904302>
- [19] Wang S, Wang A, Hao F et al (2022) 2D arsenenes. *J Semicond* 43:030201. <https://doi.org/10.1088/1674-4926/43/3/030201>
- [20] Giubileo F, Grillo A, Passacantando M et al (2019) Field emission characterization of MoS₂ nanoflowers. *Nanomaterials* 9:717. <https://doi.org/10.3390/NANO9050717>
- [21] Di Bartolomeo A, Grillo A, Urban F et al (2018) Asymmetric Schottky contacts in bilayer MoS₂ field effect transistors. *Adv Funct Mater* 28:1800657. <https://doi.org/10.1002/ADFM.201800657>
- [22] Guan Y, Yao H, Zhan H et al (2021) Optoelectronic properties and strain regulation of the 2D WS₂/ZnO van der Waals heterostructure. *RSC Adv* 11:14085–14092. <https://doi.org/10.1039/D1RA01877A>
- [23] Wang Q, Zhang Q, Luo X et al (2020) Optoelectronic properties of a van der Waals WS₂ monolayer/2D perovskite vertical heterostructure. *ACS Appl Mater Interfaces* 12:45235–45242
- [24] Yang T, Zheng B, Wang Z et al (2017) Van der Waals epitaxial growth and optoelectronics of large-scale WSe₂/SnS₂ vertical bilayer p–n junctions. *Nat Commun* 8:1–9
- [25] Di Bartolomeo A, Pelella A, Urban F et al (2020) Field emission in ultrathin PdSe₂ back-gated transistors. *Adv Electron Mater* 6:2000094. <https://doi.org/10.1002/AELM.202000094>
- [26] Pelella A, Grillo A, Urban F et al (2021) Gate-controlled field emission current from MoS₂ nanosheets. *Adv Electron Mater* 7:2000838. <https://doi.org/10.1002/AELM.202000838>
- [27] Zeng M, Xiao Y, Liu J et al (2018) Exploring two-dimensional materials toward the next-generation circuits: from monomer design to assembly control. *Chem Rev* 118:6236–6296
- [28] He Q, Liu Y, Tan C et al (2019) Quest for p-type two-dimensional semiconductors. *ACS Nano* 13:12294–12300
- [29] Grillo A, Di Bartolomeo A, Urban F et al (2020) Observation of 2D conduction in ultrathin germanium arsenide field-effect transistors. *ACS Appl Mater Interfaces* 12:12998–13004
- [30] Di Bartolomeo A (2016) Graphene Schottky diodes: an experimental review of the rectifying graphene/semiconductor heterojunction. *Phys Rep* 606:1–58. <https://doi.org/10.1016/J.PHYSREP.2015.10.003>
- [31] Xu Y, Shi Z, Shi X et al (2019) Recent progress in black phosphorus and black-phosphorus-analogue materials: properties, synthesis and applications. *Nanoscale* 11:14491–14527. <https://doi.org/10.1039/C9NR04348A>
- [32] Li P, Lu J, Cui H et al (2021) The development, application, and performance of black phosphorus in energy storage and conversion. *Mater Adv* 2:2483–2509. <https://doi.org/10.1039/D0MA01016B>
- [33] Tahir MB, Fatima N, Fatima U, Sagir M (2021) A review on the 2D black phosphorus materials for energy applications. *Inorg Chem Commun* 124:108242. <https://doi.org/10.1016/J.INOCHE.2020.108242>
- [34] Eswaraiiah V, Zeng Q, Long Y, Liu Z (2016) Black phosphorus nanosheets: synthesis, characterization and applications. *Small* 12:3480–3502. <https://doi.org/10.1002/SMLL.201600032>
- [35] Huang S, Ling X (2017) Black phosphorus: optical characterization, properties and applications. *Small* 13:1700823. <https://doi.org/10.1002/SMLL.201700823>
- [36] Wang CH, Incorvia JAC, McClellan CJ et al (2018) Unipolar n-type black phosphorus transistors with low work function contacts. *Nano Lett* 18:2822–2827
- [37] Wang L, Liao W, Xu S et al (2019) Unipolar n-type conduction in black phosphorus induced by atomic layer deposited MgO. *IEEE Electron Device Lett* 40:471–474. <https://doi.org/10.1109/LED.2019.2895678>
- [38] Zhu W, Yogeesh MN, Yang S et al (2015) Flexible black phosphorus ambipolar transistors, circuits and AM demodulator. *Nano Lett* 15:1883–1890. <https://doi.org/10.1021/nl5047329>
- [39] Tian H, Deng B, Chin ML et al (2016) A dynamically reconfigurable ambipolar black phosphorus memory device. *ACS Nano* 10:10428–10435
- [40] Feng Q, Yan F, Luo W, Wang K (2016) Charge trap memory based on few-layer black phosphorus. *Nanoscale* 8:2686–2692. <https://doi.org/10.1039/C5NR08065G>
- [41] Grillo A, Pelella A, Faella E et al (2021) Memory effects in black phosphorus field effect transistors. *2D Mater* 9:015028. <https://doi.org/10.1088/2053-1583/AC3F45>

- [42] Wei Q, Peng X (2014) Superior mechanical flexibility of phosphorene and few-layer black phosphorus. *Appl Phys Lett* 104:251915. <https://doi.org/10.1063/1.4885215>
- [43] Teng F, Hu K, Ouyang W, Fang X (2018) Photoelectric detectors based on inorganic p-type semiconductor materials. *Adv Mater* 30:1706262. <https://doi.org/10.1002/ADMA.201706262>
- [44] Lee CH, Lee GH, Van Der Zande AM et al (2014) (2014) Atomically thin p–n junctions with van der Waals heterointerfaces. *Nat Nanotechnol* 9(9):676–681. <https://doi.org/10.1038/nnano.2014.150>
- [45] Low T, Engel M, Steiner M, Avouris P (2014) Origin of photoresponse in black phosphorus phototransistors. *RAPID Commun Phys Rev B* 90:81408. <https://doi.org/10.1103/PhysRevB.90.081408>
- [46] Liu S, Huo N, Gan S et al (2015) Thickness-dependent Raman spectra, transport properties and infrared photoreponse of few-layer black phosphorus. *J Mater Chem C* 3:10974–10980. <https://doi.org/10.1039/c5tc01809a>
- [47] Borah CK, Tyagi PK, Kumar S, Patel K (2018) Few-layer p-type phosphorene sheet: an efficient transparent conducting electrode in silicon heterojunction solar cell. *Comput Mater Sci* 151:65–72. <https://doi.org/10.1016/J.COMMATSCI.2018.04.059>
- [48] Favron A, Gaufrès E, Fossard F et al (2014) Photooxidation and quantum confinement effects in exfoliated black phosphorus. *Nat Mater* 14(14):826–832. <https://doi.org/10.1038/nmat4299>
- [49] Tan WC, Wang L, Feng X et al (2019) Recent advances in black phosphorus-based electronic devices. *Adv Electron Mater* 5:1800666. <https://doi.org/10.1002/AELM.201800666>
- [50] Kastuar SM, Ekuma CE, Liu ZL (2022) Efficient prediction of temperature-dependent elastic and mechanical properties of 2D materials. *Sci Rep* 12:1–8. <https://doi.org/10.1038/s41598-022-07819-8>
- [51] Polfus JM, Muñoz MB, Ali A et al (2021) Temperature-dependent adhesion in van der Waals heterostructures. *Adv Mater Interfaces* 8:2100838. <https://doi.org/10.1002/ADMI.202100838>
- [52] Zhang L, Tang Y, Raza Khan A et al (2020) 2D materials and heterostructures at extreme pressure. *Adv Sci* 7:2002697. <https://doi.org/10.1002/ADVS.202002697>
- [53] Faella E, Intonti K, Viscardi L et al (2022) Electric transport in few-layer ReSe₂ transistors modulated by air pressure and light. *Nanomaterials* 12:1886. <https://doi.org/10.3390/NANO12111886>
- [54] Pei S, Wang Z, Xia J (2022) High pressure studies of 2D materials and heterostructures: a review. *Mater Des* 213:110363. <https://doi.org/10.1016/J.MATDES.2021.110363>
- [55] Yang S, Chen Y, Jiang C (2021) Strain engineering of two-dimensional materials: methods, properties, and applications. *InfoMat* 3:397–420. <https://doi.org/10.1002/INF2.12177>
- [56] Di Bartolomeo A, Genovese L, Giubileo F et al (2017) Hysteresis in the transfer characteristics of MoS₂ transistors. *2D Mater* 5:015014. <https://doi.org/10.1088/2053-1583/AA91A7>
- [57] Urban F, Martucciello N, Peters L et al (2018) Environmental effects on the electrical characteristics of back-gated WSe₂ field-effect transistors. *Nanomaterials* 8:901. <https://doi.org/10.3390/NANO8110901>
- [58] Urban F, Giubileo F, Grillo A et al (2019) Gas dependent hysteresis in MoS₂ field effect transistors. *2D Mater* 6:045049. <https://doi.org/10.1088/2053-1583/AB4020>
- [59] Di Bartolomeo A, Pelella A, Liu X et al (2019) Pressure-tunable ambipolar conduction and hysteresis in thin palladium diselenide field effect transistors. *Adv Funct Mater* 29:1902483. <https://doi.org/10.1002/ADFM.201902483>
- [60] Wu J, Koon GKW, Xiang D et al (2015) Colossal ultraviolet photoresponsivity of few-layer black phosphorus. *ACS Nano* 9:8070–8077
- [61] Feng X, Huang X, Chen L et al (2018) High mobility anisotropic black phosphorus nanoribbon field-effect transistor. *Adv Funct Mater* 28:1801524. <https://doi.org/10.1002/ADFM.201801524>
- [62] Ricciardulli AG, Wang Y, Yang S, Samori P (2022) Two-dimensional violet phosphorus: a p-type semiconductor for (opto)electronics. *J Am Chem Soc* 144:3660–3666
- [63] Brown WD, Brewer J (1998) Nonvolatile semiconductor memory technology: a comprehensive guide to understanding and to using NVSM devices. *IEEE*, New York, p 590
- [64] Di Bartolomeo A, Yang Y, Rinzan MBM et al (2010) Record endurance for single-walled carbon nanotube-based memory cell. *Nanoscale Res Lett* 5:1852. <https://doi.org/10.1007/s11671-010-9727-6>
- [65] Youngblood N, Li M (2017) Ultrafast photocurrent measurements of a black phosphorus photodetector. *Appl Phys Lett* 110:051102. <https://doi.org/10.1063/1.4975360>
- [66] Gong F, Wu F, Long M et al (2018) Black phosphorus infrared photodetectors with fast response and high photoresponsivity. *Phys Status Solidi Rapid Res Lett* 12:1800310. <https://doi.org/10.1002/PSSR.201800310>
- [67] Buscema M, Groenendijk DJ, Blanter SI et al (2014) Fast and broadband photoresponse of few-layer black phosphorus field-effect transistors. *Nano Lett* 14:3347–3352
- [68] Liu Y, Cai Y, Zhang G et al (2017) Al-doped black phosphorus p–n homojunction diode for high performance

- photovoltaic. *Adv Funct Mater* 27:1604638. <https://doi.org/10.1002/ADFM.201604638>
- [69] Youngblood N, Chen C, Koester SJ, Li M (2015) Waveguide-integrated black phosphorus photodetector with high responsivity and low dark current. *Nat Photonics* 9(9):247–252. <https://doi.org/10.1038/nphoton.2015.23>
- [70] Abderrahmane A, Woo C, Ko PJ (2021) Black phosphorus/molybdenum diselenide heterojunction-based photodetector. *J Electron Mater* 50:5713–5720
- [71] Sharma M, Aggarwal P, Singh A et al (2022) Flexible, transparent, and broadband trilayer photodetectors based on MoS₂/WS₂ nanostructures. *ACS Appl Nano Mater* 5:13637–13648. <https://doi.org/10.1021/ACSANM.2C03394>
- [72] Zou Y, Zhang Z, Yan J et al (2022) High-temperature flexible WSe₂ photodetectors with ultrahigh photoresponsivity. *Nat Commun* 13(13):1–9. <https://doi.org/10.1038/s41467-022-32062-0>
- [73] Ye P, Xiao H, Zhu Q et al (2022) Si-CMOS-compatible 2D PtSe₂-based self-driven photodetector with ultrahigh responsivity and specific detectivity. *Sci China Mater* 2022:1–9. <https://doi.org/10.1007/S40843-022-2119-1>
- [74] Li K, Du C, Gao H et al (2022) Ultrafast and polarization-sensitive ReS₂/ReSe₂ heterostructure photodetectors with ambipolar photoresponse. *ACS Appl Mater Interfaces* 14:33589–33597. <https://doi.org/10.1021/ACSAMI.2C09674>
- [75] Grillo A, Faella E, Pelella A et al (2021) Coexistence of negative and positive photoconductivity in few-layer PtSe₂ field-effect transistors. *Adv Funct Mater* 31:2105722. <https://doi.org/10.1002/ADFM.202105722>
- [76] Zhou F, Chen J, Tao X et al (2019) 2D materials based optoelectronic memory: convergence of electronic memory and optical sensor. *Research* 2019:1–17. <https://doi.org/10.34133/2019/9490413>
- [77] Chen C, Chen F, Chen X et al (2019) Bright mid-infrared photoluminescence from thin-film black phosphorus. *Nano Lett* 19:1488–1493

Publisher's Note Springer Nature remains neutral with regard to jurisdictional claims in published maps and institutional affiliations.